Mathematical Modeling of a Biological Odometry

Somayeh Danafar (somayeh@idsia.ch)
Istituto Dalle Molle di Studi sull'Intelligenza Artificiale (IDSIA),
Galleria 2, Manno-Lugano, 6928, Switzerland

Abstract

Flexible and robust biological navigation are role models for robots. Biological odometry data from experiments with human subjects are explained by our novel mathematical model of biological path integration. We show the equivalence of neural representations of Polar and Cartesian egocentric path integration.

Keywords: Odometry; Path integration; Egocentric; Mathematical modeling.

1 Introduction

Navigation can be defined as a process that answers the following questions (a) "where am I?" (b) "where are other places with respect to me?" (c) "how do I get to other places with respect to me?" (Levitt and Lawton, 1990). Navigation is different from other forms of spatial behavior such as exploration, or foraging, in that there is an explicit reference to a goal location (Franz & Mallot, 2000). While many animals normally use landmarks or familiar positions to navigate, arthropods, many mammals and humans can reach their goal relying solely on their own locomotion signals. This type of navigation is known as *path integration* in biology or *odometry* in robotics.

Path integration has been studied extensively in desert arthropods and mammals (Weber et al., 1997; Séguinot et al., 1998; Etienne & Jeffery, 2004; Merkle, 2007). For humans, path integration is normally studied through triangle completion experiments (e.g. Riecke et al.). Wiener and Mallot (2006) studied visual path integration on human subjects using more complex paths with a greater number of segments and turning angles.

In robotics, sensory inputs are used to build and update a global representation of the environment. Thereafter, motor actions are derived by an inference procedure from this representation (McKerrow, 1991). The flexibility and navigation performance of biological organisms (e.g. migrating birds, arthropods) has motivated robotics researchers to adopt biologically-inspired approaches in order to achieve more accurate and robust navigation. Viewed in the opposite direction, such robots can help us to understand the behavior and biomechanics of biological systems. For instance, Möller et al. (1998) used an autonomous agent to study path integration in a type of desert ant. Lambrinos et al. (1997) studied the encoded signals of robot's wheels to estimate the moved distance. Polarized light was used as an allothetic signal. The navigation ability of a mobile robot using only visual sensory input was investigated by Chahl and Srinivasan (1996). Weber et al. (1997) studied image motion information to estimate the travelled distance by the robot.In this paper, we address the problem of odometry through the mathematical modeling of a path integration system which matches the results from experiments conducted on human subjects (Riecke et al., 2002). In this way, we investigate what is happening at the neuronal level during the execution of the task which can later be used in biomimetic robots.

Generally speaking mathematical models of path integration can be divided in two types: geocentric and egocentric. In the present work, we focus on the egocentric model, described in section 2.1. Section 2.2 defines different sources of noise that arise in path integration. In section 2.3. the experimental data obtained from path integration with human subjects is described. In section 2.4 the mathematical model of this system is explained. To find the noise parameters which define the best mathematical model according to the experimental data, we need to solve an optimization problem which we elaborate on in section 3. The results are provided in section 4.

2 Path Integration (Odometry)

Mittelstaedt and Mittelstaedt (1980) established the term "path integration" and were the first to study it from a computational standpoint. They hypothesized that the signals derived from locomotion are used continuously to estimate the so-called global vector (travelled distance). This vector connects the reference point (e.g. the nest position) to the current position of the agent (e.g. the goal or target point) in a fixed coordinate system. These models of path integration are known as *Geocentric models.*

In contrast, *Egocentric models* center the coordinate system on the body of the moving agent. The agent computes and updates the sensory signals pertaining to its position and orientation in each time step (Gallistel, 1990; Benhamou and Séguinot, 1995). This approach is computationally efficient and particularly important in e.g. ants, given their limited computational resources.

Both models can be defined in terms of Polar and Cartesian coordinates. The models investigated here are based on an egocentric computation to formulate the path integration task conducted in an experiment on human subjects.

2.1 Egocentric Models

For path integration in egocentric models, two velocities are measured, the forward (translational) velocity, *v*, and the angular velocity, ω (Figure 1). Egocentric related differential equations formulated by Banhamou and Séguinot (1995) are obtained considering small time steps. In the polar coordinates they are,

$$\frac{dr}{dt} = -v\cos\delta, \quad (1)$$

$$\frac{d\delta}{dt} = v\frac{\sin\delta}{r} - \omega. \quad (2)$$

The differential equations in Cartesian coordinates (by Banhamou and Séguinot , 1995) are,

$$\frac{dx}{dt} = -v + \omega y, \quad (3)$$

$$\frac{dy}{dt} = -\omega x. \quad (4)$$

This egocentric model linearly applies the parameters *v*, and ω, as additive or multiplicative terms.

2.2 Noise Type

Homing in mammals and arthropods is imperfect. The lack of familiar positions or salient objects in identifying the starting position produces errors during path integration (Riecke et al., 2002). There are two types of errors in path integration that should be distinguished: random and systematic errors. Merkle (2007) mentioned that "there is evidence that random errors can originate from the inaccurate measurement of angles or distances, whereas systematic errors probably arise at the neural level of the organism".

We examine the effect of both types of noise in path integration which is modelled by Monte-Carlo simulation in each unit of path movement. The first type of noise affects the sensors which measure *v* and ω. This is considered due to the imperfectness of sensors. As the agent moves, it uses path integration to update its position across movement steps in relation to the reference point (nest position). The second type of noise is added to these calculated values to obtain the agent's position (Figure 2).

2.3 Experimental Data

To examine whether only vestibular cues are required for navigation, Riecke et al. (2002) conducted experiments on spatial orientation tasks. The experiments were conducted in the 180˚ Virtual Reality (VR) environment lab, with a half-cylindrical screen, where the participant is seated behind a

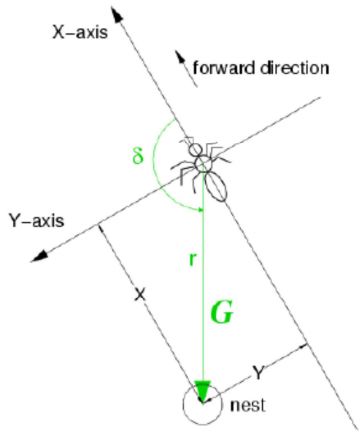

Figure 1: Egocentric path integration schema. The global vector, G, represented in Cartesian coordinates as G =(X, Y), and the polar coordinates G=(r,δ) (Merkle, 2007).

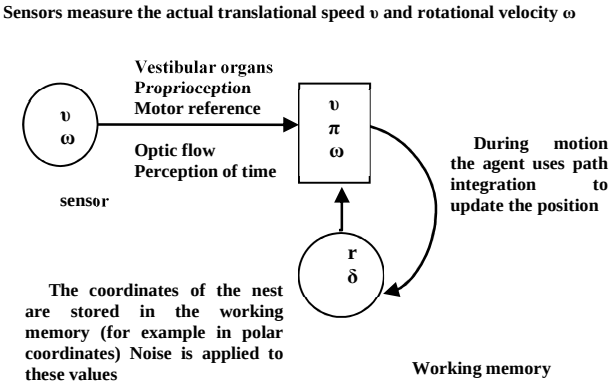

Figure 2: The types of noise in the navigation system.

table in the centre of the screen with a three button mouse , and is presented with visual cues. Pressing the middle button was used for forward translation and releasing for ending the motion. The left and right buttons were used for left or right rotations, respectively. Since there is minimum proprioceptive feedback in the button-based motion model, it is normally used as a model in VR related tasks. The experimental landscapes were streets, trees and houses. In each trial participants were presented with yellow and blue light beams, respectively, as the first and the second goal. The goals disappeared on contact. After the second goal disappeared there was a 2 second period of darkness. The task was then to return to the starting position accurately. The experiment was also done without reliable landmarks in a 3D field of blobs and with the naturalistic town environment and temporal landmarks. The reader is referred to Reicke et al. (2002) for a more detailed description.

Reicke et al. (2002) chose triangle completion since this task is "the simplest nontrivial combination of translations and rotations". Each participant was presented with sixty isosceles triangles in random order; five different turning

angles (30˚, 60˚, 90˚, 120˚, and 150˚) and two turning directions (left or right) which were repeated six times. Experimental results showed that participants could use their proprioceptive signals to estimate their travelled distance and turn back to the starting point with some bias (Figure 3). If we look at the homing trajectory end points for each participant over all his/her trials in Figure 3, we end up with a distribution over these sets of end points. We mainly work with this distribution in the next sections.

3 Mathematical Modeling

As in the experiment above, we model movement along isosceles triangles with 20 units and five different rotation angles between equal sides of a triangle. After passing one side of a triangle and reaching the first goal, the agent rotates and crosses the second side to reach the second goal and now it has to compute the third side of triangle. We used Monte Carlo simulations to simulate the path integration equations of section 2.1 and the noise of section 2.2. Sensor noise was added by Monte Carlo simulation as follows:

$$\nu' = \nu + N(\alpha_1 |\nu| + \alpha_2 |\omega|), \quad (5)$$

$$\omega' = \omega + N(\alpha_3 |\nu| + \alpha_4 |\omega|), \quad (6)$$

where ν' and ω' are the noisy sensor values, and α_1, α_2, α_3 and α_4 are user-defined free parameters.

The second type of noise was added to the calculated parameters which define the position of the agent in Polar or Cartesian coordinate systems. The noise can be added by Monte Carlo simulation in two ways: in a partial form, eqs. 7, 8 (Cartesian coordinates), 9 and 10 (Polar coordinates),

$$X' = X + N(\sigma).X \quad (7)$$

$$Y' = Y + N(\sigma).Y \quad (8)$$

$$r' = r + N(\sigma).r \quad (9)$$

$$\delta' = \delta + N(\sigma).\delta \quad (10)$$

or in an absolute form, eqs. 11, 12 (Cartesian coordinates), 13 and 14 (Polar coordinates).

$$X' = X + N(\sigma) \quad (11)$$

$$Y' = Y + N(\sigma) \quad (12)$$

$$r' = r + N(\sigma) \quad (13)$$

$$\delta' = \delta + N(\sigma) \quad (14)$$

Tuning the noise parameters of the Monte Carlo simulation yields different ending distributions around the reference point of the modelled triangular path. To evaluate the simulated results predicted by the mathematical model and the real experimental data, we compared the home-ending distributions by means of a Homogeneity test (section 3.1). Determining the best noise parameter that provides the distribution closest to the real home-ending distribution of experimental data required solving an optimization problem (section 3.2). An example simulated path from our mathematical model, and the home-ending distributions are depicted in Figure 4.

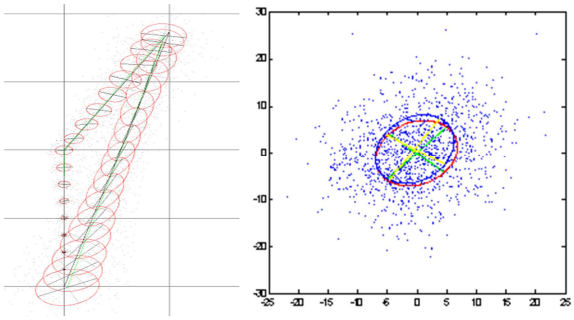

Figure 4: **L**eft: Monte Carlo simulation generated noise. The agent's rotation angle of the agent is 45 degrees. Right: the red ellipse indicates the home-ending distribution of experimental data, the blue ellipse is the one obtained by Monte Carlo simulation.

3.1 Homogeneity Testing to Compare the Distributions

Suppose $\{x_1, \ldots, x_m\}$ and $\{y_1, \ldots, y_n\}$ are two-samples drawn i.i.d. from distributions P and Q, respectively, a two-sample test tests whether $P \neq Q$ (hypotheses are, H_0: P=Q, against the alternative H_1: $P \neq Q$). We used Maximum Mean Discrepancy (MMD; Gretton et al., 2007) as our homogeneity test.

Theorem1. *Let (X,B) be a metric space, and let P, and Q be two Borel probability measures defined on X. The kernel function k: X× X→ R embeds the points* $x \in X$ *into the corresponding reproducing kernel Hilbert space H. Then P = Q if and only if MMD[P,Q] =0, where*

$$\mathrm{MMD}[P,Q] := \left\| E_p[k(x,.)] - E_Q[k(y,.)] \right\|_H,$$

where $\| \cdot \|_H$ *represents the RKHS norm.*

For a predefined significance level (e.g. 5%), MMD values closer to zero indicate higher similarity between the distributions.

3.2 Optimization

To find the noise parameters providing the modeled distribution closest to real home-ending distributions, we need to solve an optimization problem,i.e. find the maxima or minima of a so-called objective function. If the objective function is differentiable, we can use derivative-based methods to solve the optimization problem. Direct search methods are used in cases in which we do not have explicit information about the objective function, or are unable to compute the derivatives. The Nelder-Mead simplex method (Lagarias et al., 1998) is a direct search method which is widely used to optimize multidimensional objective functions with no constraints. We use the Nelder-Mead

simplex method since our objective function is a routine that does not have an analytical form. The input arguments of this routine are the noise parameters and the output is an MMD value. It has 6 free noise parameters (α_1, α_2, α_3, α_4, σ_x, and σ_y), e.g., of the noise which is generated for instance in a Cartesian coordination system. Without loss of generality we simplify equations 5 and 6 by setting α_1, α_2, α_3, α_4 equal to 1:

$$v' = v + N(\sigma) \quad (15)$$

$$\omega' = \omega + N(\sigma) \quad (16)$$

Then our goal is minimization of the simplified objective function f (σ_v, σ_ω, σ_x, σ_y) under the constraints of non-negative parameters (standard deviations). The solution is the minimal MMD values. As mentioned before, the Nelder-Mead simplex method is used to solve unconstrained problems; then, we need to convert our constrained problem to an unconstrained one. This is done with the algorithm introduced by J. D'Errico which uses the transformation values related to each bound, such as a quadratic function for ingle bounds and a sinusoidal function for dual bounds.

4 Results

To make sure our objective function is not affected by sudden unexpected changes due to changing noise parameters, we approximately cover the variable space by changing steps of 0.01 to plot the function values (Table 1). To get a smoothly changing objective function we tuned the triangular side lengths to 20 meters. This value is 40 m in real experiments. There are 1000 Monte Carlo-generated home-ending data points. For MMD we use the Gaussian kernel with automated standard deviation tuning by the median sample data distance in distributions. We report results for the 5% significance level. Results for relative noise (eq. 7 and 8) and absolute noise (eq. 11 and 12) are obtained in both Cartesian and Polar coordinate systems. Results of simulated distributions in polar coordinates with absolute noise are depicted in Figure 5. Table 2 and 3 compare simulated distributions around the reference point of the navigation path with the distribution of home-ending points in experimental data for absolute and relative noise types.

An interesting question is whether polar or Cartesian coordinates are used on the neural level. Our results show they provide similar results. We also generated final distributions compatible with experimental data.

5 Conclusion

We introduced a novel mathematical model of egocentric path integration that uses Monte Carlo simulation of both the path integration equation and the noise. The home-ending distributions of data collected from experiments with human subjects were compared to those predicted by Monte Carlo. The closest matching distribution simulated by the model was found using the Nelder-Mead simplex method to minimize the Maximum Mean discrepancy between the model and human data. We showed that at the neuronal level, the perceived advantage, in terms of both computational overhead and representational power, between Polar and Cartesian representations, is non-existent.

6 Acknowledgments

I want to thank Prof. H.A. Mallot, Prof. J. Schmidhuber, Dr. K. Basten, Dr. F. Gomez, and M. Aschoff for the profound discussions and help to prepare this paper.

7 References

Benhamou, S., & Séguinot, V. (1995). How to Find One's way in the Labyrinth of Path Integration Models. *In Biol.*,174, 463-466. (Ed.) Theor, J.

Chahl, J.S., & Srinivasan, M.V. (1996). Visual Computation of Egomotion Using an Image Interpolation Technique. *Biological Cybernetics*, 74(5), 405-411.

D'Errico, J. The Fminsearch bound, available at: http://www.mathworks.com/matlabcentral/fileexchange/authors/679.

Etienne, A.S., & Jeffery, K.J. (2004). Path Integration in Mammals. In Hippocampus.,14(2), 180-192.

Franz, M.O., & Mallot, H.A. (2000). Biomimetic Robot Navigation. *In Elsevier*, *Robotics and Autonomous Systems*, 30, 133-153.

Gallistel, C.R. (1990). The organization of learning. *In Cambridge, MA: Bradford books, MIT press.*

Gretton, A. Borgwardt, K.M., Rasch, M., Smola, A., & Schölkopf, B. (2007). A Kernel Method for the two-sample problem. *In Advances in Neural Information Processing Systems*, 19, 513-520. (Eds.) Schölkopf, B., Platt, J., Hoffman, T., MIT Press, Cambridge, MA, USA.

Lagarias, J.C., Reeds, J.A., Wright, M.H., & Wright, P.E. (1998). Convergence Properties of the Nelder-Mead Simplex Method in Low Dimensions. *In SIAM Journal of Optimization, 9*, 112-147.

Lambrinos, D., Kobayashi, H., Pfeifer, R., Maris, M., Labhart, T., & Wehner, R. (1997). An Autonomous Agent Navigation with a Polarized Light Compass. *In Adaptive Behavior*, 6, 131-161.

Levitt, T.S. & Lawton, D.T. (1990). Qualitative Navigation for Mobile Robots. *In Artificial Intelligence*, 44, 305-360.

McKerrow, P.J. (1991). Introduction to Robotics. *Addison Wesly, New-York.*

Merkle, T. (2007). Orientation and Search Strategies of Desert Arthropods: Path Integration Models and Experiments with Desert Ants, Cataglyphis Fortis (Forel 1902). *Dissertation for PhD, University of Bonn.*

Mittelstaedt, M.L., & Mittelstaedt, H. (1980) Homing by Path Integration. *In Avian Navigation*, 290-297 (Eds.) Papi, F. Wallraff, H.G., Springer, Berlin.

Möller, R., Lambrinos, D., Pfeifer, R, Labhart, T., Wehner, R. (1998) Modeling Ant Navigation with an Autonomous Agent. *In Proc. 5th Conference of Simulation of adaptive behavior.*

Riecke, B.E., Van Veen, H.A.C., & Bülthoff, H.H. (2002). Visual Homing is Possible Without Landmarks: a Pass Integration Study in Virtual Reality. *In Presence MIT*, 11 (5), 443-473.

Séguinot, V., Cattet, J., & Benhamou, S. (1998). Path Integration in Dogs. *In Animal Behavior*, 55, 787-797.

Weber, K. Venkatesh, S., & Srinivasan, M.V. (1997). Insect Inspired Behaviors for the Autonomous Control of Mobile Robots. *In From Living Eyes to Seeing Machines*.

(Eds.) Srinivasan, M.V., Verkantesh, S. Oxford University Press, Oxford, 226-248.

Wiener, J.M., and Mallot, H.A. (2006). Path Complexity Does not Impair Visual Path Integration. *Spatial cognition and computation*, 6(4), 333-346.

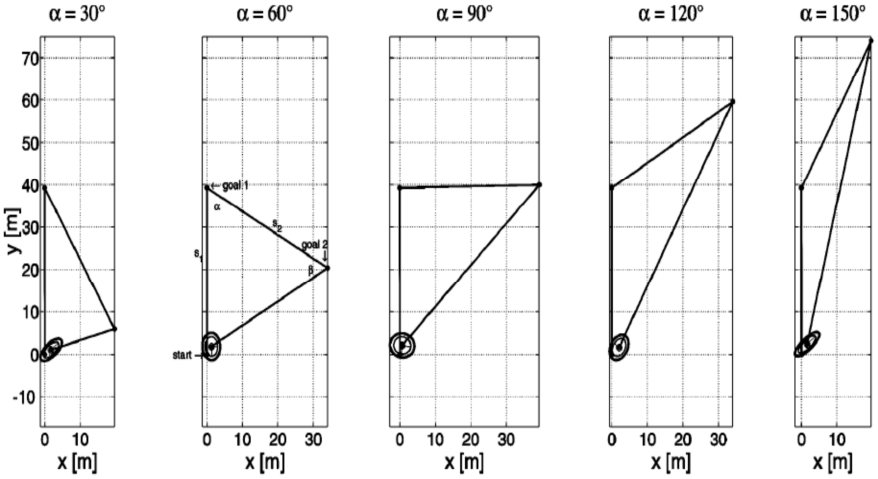

Figure 3**.** Homing performance in the Landmarks experiment. The data is pooled over the turning direction (left/right) as it had no significance influence on homing performance. Plotted are the mean (centroid), the 95% confidence ellipse (outer ellipse with thick line), and the standard ellipse (inner ellipse with thin line) for the homing endpoints (Reicke et al, 2002).

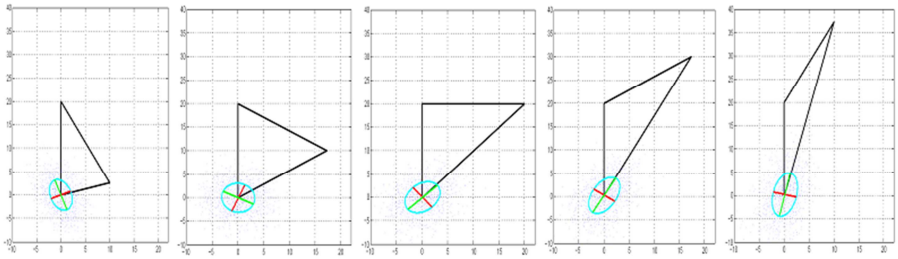

Figure 5: The results of sensor noise with absolute standard deviation production in the polar coordinate system.

Table 1: An example of how the home-ending distributions change with respect to the parameters of the Monte Carlo simulation. Entries are shown for increments of 0.01 for both σ_x, σ_y, in Cartesian coordinates. Note how the generated Monte Carlo distributions change smoothly with σ_1, σ_2. The confidence interval over 30 runs is reported. The rotation angle of the path is 120˚.

σ_x / σ_y	**0.01** σ_1, σ_2	**0.02** σ_1, σ_2	**0.03** σ_1, σ_2	**0.04** σ_1, σ_2	**0.05** σ_1, σ_2
0.01	1.63±0.01,0.77±0.01	3.24±0.02,1.55±0.03	4.77±0.02,2.37±0.03	6.26±0.05,3.28±0.02	7.66±0.1,4.21±0.08
0.02	1.63±0.03,0.77±0.01	3.27±0.03,1.56±0.01	4.77±0.01,2.37±0.02	6.32±0.06,3.30±0.02	7.65±0.13,4.23±0.03
0.03	1.64±0.01,0.79±0.01	3.27±0.03,1.59±0.03	4.75±0.10,2.37±0.01	6.28±0.02,3.29±0.08	7.61±0.15,4.25±0.08
0.04	1.65±0.02,0.81±0.02	3.24±0.04,1.59±0.04	4.78±0.06,2.38±0.04	6.25±0.09,3.21±0.08	7.61±0.11,4.22±0.05
0.05	1.64±0.03,0.81±0.01	3.25±0.06,1.60±0.02	4.80±0.11,2.40±0.06	6.27±0.06,3.25±0.05	7.64±0.10,4.32±0.05

Table 2: Comparison between simulated distributions around the initial point of the navigation path (Cartesian coordinates, various noise types). The σ_x,and σ_y to generate the Monte Carlo distributions are 0.1 and 1.6 respectively. The null hypothesis H_0, means the two distributions are similar.

Rotation Angel	**Simulated dist. Cartesian** $(\mu_x, \sigma_x, \mu_y, \sigma_y)$	**Simulated dist. Polar** $(\mu_x, \sigma_x, \mu_y, \sigma_y)$	**MMD**
30˚	0.12, 2.41,0.09,3.29	-0.04,2.36,0.02,3.28	σ = 3.3 Accept H_0
60˚	0.09,3.29,-0.01,3.09	0.06,3.22,-0.07,3.08	σ = 3.72 Accept H_0
90˚	-0.01, 3.42,-.09,3.37	0.18,3.42,-0.03,3.31	σ = 3.89 Accept H_0
120˚	0.12,3.11, 0.15,3.79	0.05,3.11,0.24,3.89	σ = 3.95 Accept H_0
150˚	-0.06,2.60,-0.01,4.51	0.15,2.54,0.19,4.66	σ = 4.10 Accept H_0

Table 3**:** Comparison of simulated distributions around the initial point of the navigation path (polar coordinates, various noise types). The σ_x, and σ_y to generated the Monte Carlo distributions are both 0.01. The null hypothesis H_0, means the two distributions are similar.

Rotation Angel	**Simulated dist. Cartesian** $(\mu_x, \sigma_x, \mu_y, \sigma_y)$	**Simulated dist. Polar** $(\mu_x, \sigma_x, \mu_y, \sigma_y)$	**MMD**
30˚	-0.15, 6.3, -0.21,6.50	-.05,6.55,0.19,6.31	σ = 7.59 Accept H_0
60˚	1.02, 6.82, 2.02, 5.14	0.82, 6.82,1.85,5.33	σ = 6.75 Accept H_0
90˚	0.87, 6.04, 0.86,4.19	0.29, 6.99,1,4.25	σ = 5.58 Accept H_0
120˚	0.82, 6.75, 0.75, 4.88	0.29,6.99,0.96,4.7	σ = 6.67 Accept H_0
150˚	-0.03,8.64, 0.31,8.61	-0.03, 8.76,0.27,8.7	σ = 10.23 Accept H_0